Journal of Materials Chemistry C

ROYAL SOCIETY OF CHEMISTRY

PAPER

View Article Online
View Journal | View Issue

Cite this: J. Mater. Chem. C, 2025, 13, 13184

Tuning the liquid crystal behavior of subphthalocyanines: effects of substitution, chirality, and hydrogen bonding†

Jorge Labella, *[ab] Elisa López-Serrano, [a] Jorge Labrador-Santiago, [a] Joaquín Barberá, [cd] César L. Folcia, [e] Teresa Sierra *[cd] and Tomás Torres *[afg]

Received 4th April 2025,
Accepted 20th May 2025

DOI: 10.1039/d5tc01417d

rsc.li/materials-c

Bowl-shaped aromatics that self-assemble into columnar liquid crystals (LCs) are key components for developing polarized semiconductors. However, progress in this field has been sluggish, as the limited set of available π-conjugated curved scaffolds has left structure–property relationships poorly understood. Herein the role that substitution pattern, substituent nature, and chirality play in the LC columnar organization of subphthalocyanines (SubPcs) is explored. Remarkably, it is revealed that enantiopure SubPcs exhibit a reduced tendency to form LC phases compared to their racemic counterparts, whereas higher substitution density increases flexibility within the columns, compromising coaxial alignment. Moreover, we find that the use of conformationally flexible, π-extended peripheral substituents enables efficient π–π stacking, and that the incorporation of hydrogen-bonding amide groups leads to highly stable mesophases with elevated melting points, although the mesophase remains at room temperature after thermal treatment. These trends are further rationalized through theoretical modeling. Overall, this work provides valuable synthetic and design guidelines for advancing bowl-shaped aromatics toward next-generation functional columnar liquid crystals.

Introduction

Bowl-shaped aromatics are attractive building blocks for the development of advanced functional materials and devices.[1] Due to their non-centrosymmetric structure, these derivatives possess a permanent dipole moment.[2] Consequently, assembling them in a columnar fashion can yield materials with polarization (Fig. 1a).[3] This high added-value feature makes bowl-shaped semiconductors strong candidates for designing liquid crystals (LCs) that can be unidirectionally aligned under the influence of an electric field (E field).[4] Such alignment ultimately results in electronic devices with oriented pathways for carrier transport, and thus excellent conductivity. Despite this potential, just very few studies focused on the preparation

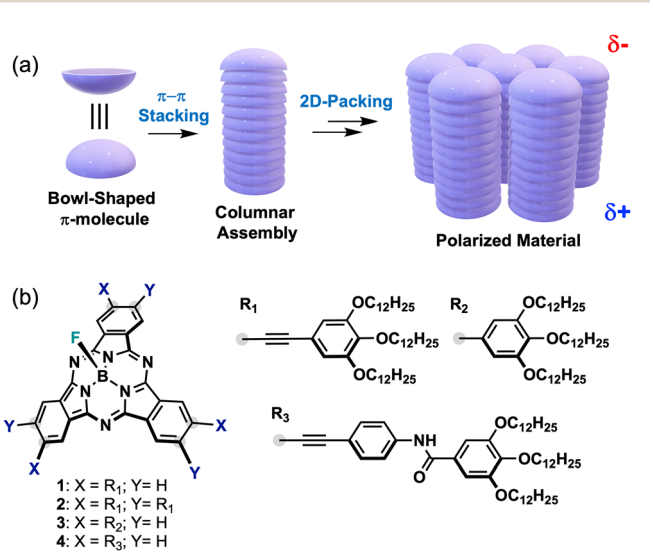

Fig. 1 (a) Schematic illustration of the head-to-tail assembly of bowl-shaped molecules and the resulting polar organization. (b) Chemical structures of the SubPcs studied in this work.

[a] Department of Organic Chemistry, Universidad Autónoma de Madrid, Campus de Cantoblanco, C/Francisco Tomás y Valiente 7, 28049 Madrid, Spain. E-mail: labella.jorge.54u@st.kyoto-u.ac.jp, tomas.torres@uam.es
[b] Department of Molecular Engineering, Kyoto University Katsura, Kyoto 615-8510, Japan
[c] Instituto de Nanociencia y Materiales de Aragón (INMA), CSIC-Universidad de Zaragoza, 50009 Zaragoza, Spain. E-mail: tsierra@unizar.es
[d] Departamento de Química Orgánica, Facultad de Ciencias, Universidad de Zaragoza, 50009 Zaragoza, Spain
[e] Department of Physics, Faculty of Science and Technology, UPV/EHU, 48940 Bilbao, Spain
[f] Institute for Advanced Research in Chemical Sciences (IAdChem), Universidad Autonoma de Madrid, 28049 Madrid, Spain
[g] IMDEA-Nanociencia, Campus de Cantoblanco, 28049 Madrid, Spain

† Electronic supplementary information (ESI) available. See DOI: https://doi.org/10.1039/d5tc01417d

of columnar LCs using concave aromatic scaffolds have been reported. This is arguably due to the challenging synthesis and peripheral functionalization of these compounds. Indeed, to the best of our knowledge, only corannulene (Cors),[4a,b] summanenes (Sums),[4d,5] and Subphthalocyanines (SubPcs)[6] have been organized into columnar mesophases. Cors and Sums have largely demonstrated exciting properties and applications. However, SubPcs display many additional features that open a broader and more realistic functional landscape.[7]

SubPcs are 14-π electron contracted aza-porphyrinoids widely employed as molecular materials in state-of-the-art areas such as molecular photovoltaics,[8] spintronics,[9] photodynamic therapy[10] and energy conversion.[11] In contrast to Cors and Sums, SubPcs display strong absorption in the visible range, which allows for implementation in optoelectronic devices. Furthermore, these macrocycles are configurationally stable due to the central boron complex, which prevents bowl-to-bowl inversion,[12] a phenomenon found in Cors and Sums.[13] This stability enables the isolation and implementation of enantiopure SubPcs in chiral technologies.[9,12] Nonetheless, SubPcs are prepared in a one-step reaction from readily accessible starting materials, and numerous methodologies have been reported for their derivatization.[7,14] Taking these attributes into account, our group and others have turned their attention to the synthesis and application of SubPc-based columnar LCs.[6] In this line, several thermotropic and lyotropic mesophases with unique properties, such as ferroelectricity,[4c] switchable polarity,[6b] or bulk-photovoltaic effect,[6a] have been developed. However, the structure–property relationship in the design of SubPc-based LCs is barely understood, since the compounds used so far are limited to trisubstituted or, eventually, hexa-thioether derivatives. Providing insights on this aspect is one of the most fundamental steps for the further advance of polarized, columnar materials.

In this work, we demonstrate how key factors, that is, chirality, substituent nature, and substitution pattern, play a crucial role in the LC behavior of SubPcs. To this end, **SubPcs 1–4** were designed to self-assemble into columnar structures, synthesized, and characterized using differential scanning calorimetry (DSC), polarized optical microscopy (POM), and X-ray diffraction (XRD). Additionally, the polarity of the resulting LCs was analyzed preliminarily through second-harmonic generation (SHG) experiments, and the structure of the assemblies was assessed through theoretical modeling. Overall, our findings reveal that chirality favors crystallization rather than promoting mesophase behavior; the presence of hydrogen bonds facilitates columnar organization but significantly increases the melting temperatures; and while a higher number of substituents enables columnar assembly, steric congestion compromises uniaxial alignment. These results offer valuable insights for the rational design of polarized semiconductors based on bowl-shaped aromatics.

Results and discussion

The molecular design of **SubPcs 1–4** relied on equipping the aromatic core with: (i) fluorine as axial ligand, to enable efficient π–π stacking and endow strong dipole moment; (ii) different peripheral groups (R_1–R_3) featuring paraffinic chains to stabilize the columnar stacking while providing flexibility. R_1 and R_2 differ in the character of the moiety linked to the SubPc (*i.e.*, alkyne of aryl), whereas R_1 and R_3 differ in the presence or absence of an amide group, which is well-known to reinforce and direct the columnar assembly. Thus, from comparison between **SubPc 1**, **3** and **4** the importance of the substituent's nature can be assessed. On the other hand, **SubPc 2** bears six peripheral groups instead of three, which allows for understanding the influence of the substitution density. It should be noted that **SubPc 2** is achiral due to its C_3v symmetry. One step further, **SubPc 1**, which is chiral (C_3 symmetry) and was previously reported as racemate (**SubPc 1RAC**),[6c] is herein described in its enantiopure form (**SubPcs 1M/P**) to reveal the role of chirality.

SubPcs 1–4 were prepared following a two-step protocol involving, first, a palladium-catalysed Sonogashira cross-coupling on either tri- or hexa-iodinated SubPcs, and second, an axial ligand exchange using $AgBF_4$. **SubPc 1M/P** was prepared similarly but starting from enantiopure triiodo-SubPcs, which were previously obtained by chiral HPLC resolution.[12] By contrast, **SubPc 3** was prepared through a methodology recently reported in our group, entailing the use of borylated-SubPcs and subsequent Suzuki–Miyaura cross-coupling reaction.[13]

The thermal properties of all the compounds were analysed by POM and DSC. Both enantiomers of **SubPc 1** behaved as crystalline solids (Fig. S3.1 and S3.3, ESI†), with melting points of 124 °C for enantiomer **SubPc 1M** and 126 °C for enantiomer **SubPc 1P**. This is in contrast to their racemic mixture (**SubPc 1RAC**), which behaves as a monotropic LC, with a lower melting point of 101 °C, and a Col_h phase stable at room temperature (RT).[6c] On cooling from the isotropic liquid under POM, and upon mechanical shearing, **SubPc 2** showed birefringence with an undefined texture (Fig. S3.2, ESI†), which revealed molecular order consistent with columnar LC behavior as confirmed by XRD (see below). According to the DSC thermogram (Fig. S3.4, ESI†), this mesophase was found to be monotropic, with a transition temperature on cooling from the isotropic liquid at *ca.* 28 °C (peak maximum). The second heating scan showed a cold crystallization (*ca.* 51 °C), followed by an endothermic peak, likely related to the transition from a crystalline phase to the isotropic liquid. Accordingly, the mesophase formed by **SubPc 2** on cooling is metastable at RT and undergoes crystallization on heating. **SubPc 3** appeared birefringent at RT (Fig. 2). Above 90 °C, the sample became slightly fluid and could be sheared. The texture developed on cooling from the isotropic liquid (147 °C) is consistent with LC behavior likely with columnar organization. The DSC thermogram (Fig. S3.5, ESI†) showed a sharp peak with onset at 135 °C and an enthalpy value of 6.1 kcal mol^{-1}. For **SubPc 4** neither POM observations nor DSC thermograms (Fig. S3.6, ESI†) were conclusive of LC behavior, although this was confirmed by XRD (see below). Between crossed polarizers, this compound appeared black on either heating or cooling, with no birefringence that would be unequivocally indicative of molecular organization. After a first heating scan in which an endothermic peak followed by an exothermic

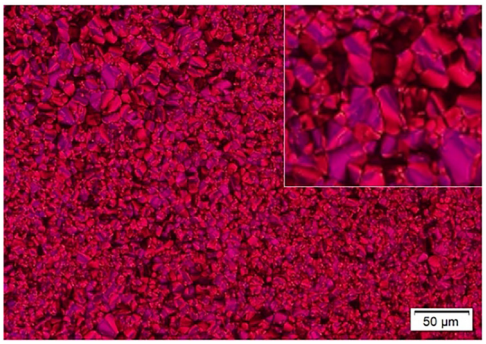

Fig. 2 Texture observed between crossed polarizers for **SubPc 3** at 28 °C upon cooling at 5 °C min^{-1} from the isotropic liquid.

one were observed, no peaks associated with first order transitions was observed in subsequent cooling–heating cycles.

Powder XRD experiments were carried out for all the compounds in order to confirm POM and DSC observations and to determine the structural parameters of the mesophases. The samples were studied at RT in the pristine (as-obtained) state and after a thermal treatment consisting of heating to a temperature above the melting point detected by DSC, followed by slow cooling. As expected, the XRD pattern of **SubPc 1M/P** was consistent with crystalline order (Fig. S3.7, ESI†), showing some characteristic features of a columnar structure, such as an intense small-angle reflection together with a clear reflection corresponding to 3.5 Å typical of a stacking distance – superimposed on a broad halo. A spacing of 39.4 Å was obtained from the intense peak, which is similar to those measured for **SubPc 2**, **3** and **4** (see below). On the other hand, the LC nature of compounds **SubPc 2–4** after thermal treatment was confirmed by the high-angle halo detected in the corresponding diffractograms (Fig. 3). This halo gives a mean distance of 4.4 Å and is related to the short-range interferences between the conformationally-disordered hydrocarbon chains, as usually found in all kinds of mesomorphic phases. The analysis of the maxima in the small-angle region allowed to determine the structure of the mesophase. For compound **SubPc 2**, the diffractogram recorded on the pristine sample is typical of a crystalline solid, although with a significant degree of disorder, as indicated by the semi-diffuse character of some X-ray maxima (Fig. S3.8, ESI†). This may be related with the coexistence of a crystalline and LC phase as suggested by the DSC results. After heating up to 85 °C and slow cooling, the diffractogram recorded (Fig. 3a) confirms the presence of the LC phase free from crystalline solid. The sharpness of the maximum at low angles and the presence of a broad, diffuse halo at high angles are consistent with a columnar mesophase, probably of hexagonal type. By applying Bragg's law to the low-angle maximum, a spacing of 37.5 Å is obtained that, assuming hexagonal symmetry, would correspond to the (1 0) reflection of the 2D lattice and gives a hexagonal lattice constant a = 43.3 Å. On the other hand, the diffractograms of **SubPc 3** recorded both on the pristine state (Fig. S3.9, ESI†) and on a thermally-treated sample (Fig. 3b) are consistent with a hexagonal columnar mesophase, although in the pristine sample the mesophase coexists with a

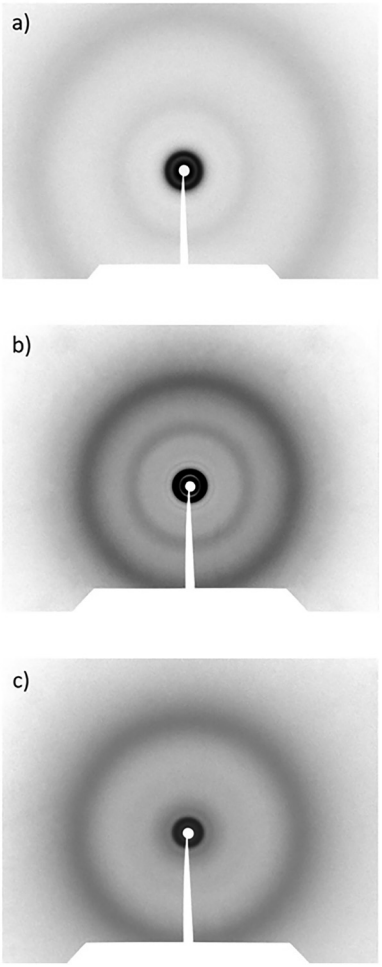

Fig. 3 DRX diffractograms of thermally treated samples of (a) **SubPc 2**, recorded at distance of 120 mm, (b) **SubPc 3**, recorded at distance of 80 mm, and (c) **SubPc 4**, recorded at a distance of 80 mm.

small proportion of crystalline phase. The two maxima observed in the low-angle region correspond to distances 31.1 Å and 18.3 Å with a reciprocal ratio $1:\sqrt{3}$, which can be indexed as the (1 0) and (1 1) reflections of a 2D hexagonal lattice, with a lattice constant a = 36.2 Å, both before and after thermal treatment. For **SubPc 4**, the diffractograms recorded on the pristine samples are characteristic of a crystalline phase, although with a high degree of disorder (Fig. S3.10, ESI†). On the other hand, the diffratograms recorded on the thermally-treated samples (Fig. 3c) are unequivocally consistent with a hexagonal columnar mesophase. Indeed, a set of two maxima are observed in the low-angle region, which correspond to distances 36.5 Å and 20.6 Å. The relationship $1:\sqrt{3}$ between these two distances allows their indexing as the (1 0) and (1 1) reflections of a 2D hexagonal lattice, respectively, and gives a lattice constant a = 41.8 Å, both before and after thermal treatment.

The hexagonal lattice constants a measured for the three LC compounds follow a size sequence **SubPc 2** > **SubPc 4** > **SubPc 3** (43.3 Å > 41.8 Å > 36.2 Å), which agrees with their corresponding molar mass, 4329.6 for **SubPc 2**, 2730.8 for **SubPc 4**, 2301.4 for **SubPc 3**. These distances, however, are

not fully consistent with the theoretical trend **SubPc 4** (53.2 Å) > **SubPc 2** (46.0 Å) > **SubPc 3** (36.8 Å) suggesting more pronounced interdigitation between the paraffinic chains in **SubPc 4**. Considering an average distance of 4.4 Å and one molecule per hexagonal unit cell, a density close to (or slightly lower than) 1 g cm^{-3}, typical or organic compounds, is estimated for all the three compounds and this supports the correct assignation of the mesophases.

In order to investigate whether the stacking of these compounds could provide spontaneous polar order, the existence of SHG was checked in compounds **SubPc 2** and **SubPc 3** in 5 nm thickness linkam cells properly oriented respect to the light incidence and polarization. No second harmonic signal was observed in the case of **SubPc 2** in the whole temperature range irrespective of the application of a bias electric field. On the other hand, for **SubPc 3** a weak SHG signal was detected under a DC electric field, which slowly increased and appeared to saturate for fields of about 10 V μm^{-1} regardless its polarity, and disappeared when removing the voltage. Accordingly, **SubPc 3** behaves as a paraelectric material, and its response occurs at the molecular level and not with the columnar organization since the response is observable also in the isotropic liquid phase.

To gain insight into the origin of this distinct supramolecular behavior observed, we performed theoretical calculations at the GFN2-xTB level (see ESI† for further details). Tetramers composed of **SubPcs 1–4** were thus optimized, with the bulky dodecyl peripheral chains replaced by propyl groups to reduce computational cost. Racemic aggregates were modelled based on heterochiral interactions, as this is the expected binding mode according to previous findings from our group.[3b,15] As shown in Fig. 4, all SubPc derivatives tend to π–π stack into the expected columnar assemblies, although notable structural differences are evident. To quantify these differences, we evaluated two parameters that characterize key aspects of columnar stacking: (i) the average B–F distance between two adjacent molecules, reflecting the π–π separation; and (ii) the average B–F–B angle formed by neighbouring units, which provides a measure of the tilting within the stack.

Remarkably, only very subtle variations in the B–F distance are observed across the different aggregates. Heterochiral binding in **SubPc 1RAC**—expected in racemic mixtures of SubPc-based supramolecular polymers[15] exhibits slightly larger B–F distances compared to the homochiral counterpart, **SubPc 1M**. Moreover, the B–F–B angle is closer to ideal coaxial alignment (180°) in the enantiopure **SubPc 1M/P** than in the racemic **SubPc 1RAC**. This points to a more compact and less flexible columnar stacking in the enantiopure form, consistent with previous findings from our group,[15] which demonstrated that heterochiral binding is entropically favoured, whereas homochiral binding is enthalpically preferred. This structural rigidity aligns with the tendency of **SubPc 1M/P** to crystallize rather than exhibit LC behaviour, although adopting columnar order with long-range stacking distance as deduced from DRX experiments (Fig. S3.7, ESI†). In the case of **SubPc 2**, although the π–π distance is comparable to that of **SubPc 1**, its tetramers show greater tilting, suggesting a reduced tendency to align coaxially along the B–F direction. This observation is in good agreement with its paraelectric rather than ferroelectric response. **SubPc 3**, on the other hand, displays good coaxial alignment and a slightly longer B–F distances compared to **SubPcs 1** and **2**. This may be attributed to its shorter peripheral branches, which form fewer π–π and van der Waals interactions than the longer, π-extended arylalkyne substituents in **SubPcs 1** and **2**. Furthermore, the peripheral aryl groups in **SubPc 3** cannot adopt the planar conformation observed in **SubPcs 1** and **2**, thereby limiting intermolecular π–π overlap. In contrast, **SubPc 4** exhibits the shortest B–F distances and nearly perfect coaxial

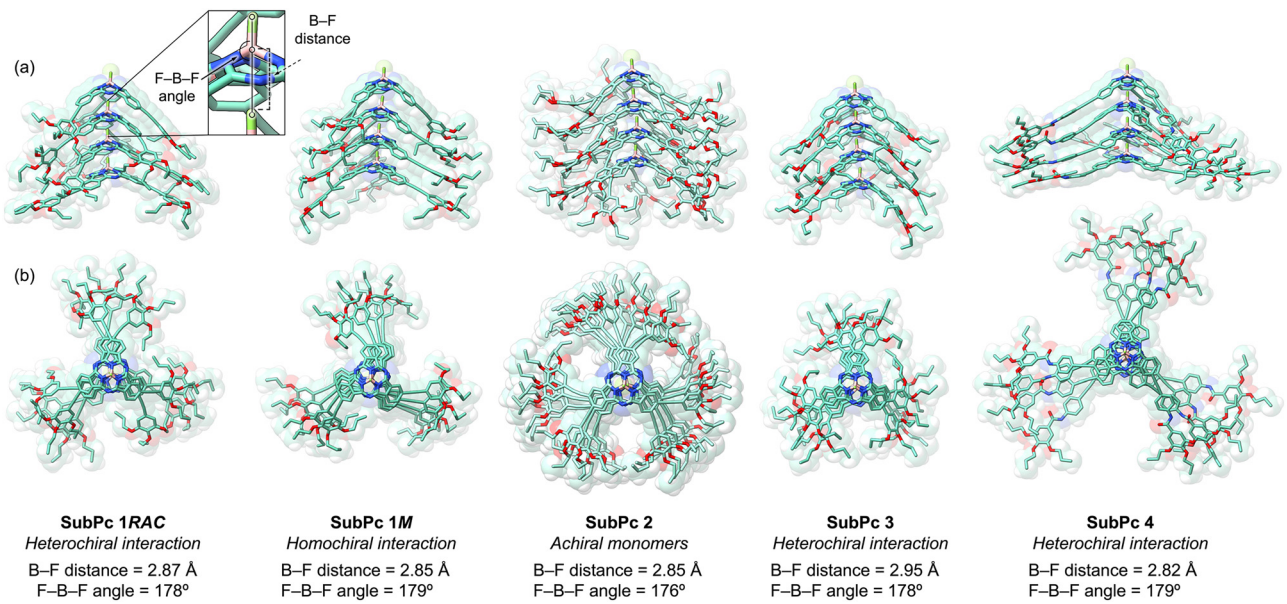

Fig. 4 (a) Side and (b) top views of the supramolecular tetramers of **SubPcs 1–4** fully optimized at the GFN2-xTB level. Atom color code: carbon in light blue, oxygen in red, nitrogen in electric blue, boron in pink, and fluorine in lime green. Hydrogen atoms are omitted for clarity.

alignment, which can be attributed to the formation of strong, highly directional hydrogen bonds. This robust SubPc–SubPc interaction is further evidenced by the pronounced terminal effect observed, defined as the difference in concavity between the isolated molecule and the terminal units within the assembly. Such tight binding in **SubPc 4** is consistent with the high temperatures required experimentally to reach the isotropic melt.

Conclusions

In summary, a series of columnar mesophases based on bowl-shaped SubPc aromatics that differ in enantiopurity, substitution nature, and substitution number have been described. The building blocks were readily synthesized from accessible precursors *via* cross-coupling reactions. Although all compounds were designed to form columnar mesophases, significant differences in their self-assembly behavior were observed. Specifically, it was found that (i) the use of enantiopure samples hinders LC behavior by promoting crystallization; (ii) increasing the number of peripheral substituents from three to six compromises coaxial alignment; (iii) peripheral alkynylaryl substituents provide an optimal balance between conformational flexibility and π–π overlap; and (iv) amide groups effectively direct columnar assembly and stabilize mesophases, although the strong hydrogen-bonding network requires high temperatures to be disrupted, thus preventing electrical alignment. Theoretical calculations support these findings by showing that enantiopure SubPcs tend to pack more tightly, hexasubstituted derivatives do not exhibit perfect coaxial alignment, and amides indeed promote strong SubPc–SubPc binding.

The structure–property relationships presented here thus offer valuable guidance for advancing columnar materials based on bowl-shaped aromatics.

Data availability

The data supporting the findings of this study is available within the article and its ESI.†

Conflicts of interest

There are no conflicts to declare.

Acknowledgements

Financial support from the Spanish MCIN/AEI/10.13039/501100011033 and European Union NextGenerationEU/PRTR (TED2021-131255B-C43), MCIU/AEI/10.13039/501100011033/FEDER, UE (PID) (PID2023-151167NB-I00, PID2021-122882NB-I00, PID2021-126132NB-I00 and PID2023-150255NB-I00), the Comunidad de Madrid and the Spanish State through the Recovery, Transformation and Resilience Plan [''Materiales Disruptivos Bidimensionales (2D)'' (MAD2D-CM) (UAM1)-MRR Materiales Avanzados], the Gobierno de Aragón- FSE (E47_23R-research group), the Basque Government project IT1458-22, and the European Union through the Next Generation EU funds is fully acknowledged. IMDEA Nanociencia acknowledges support from the ''Severo Ochoa'' Programme for Centres of Excellence in R&D (MINECO, CEX2020-001039-S). INMA acknowledges support from the ''Severo Ochoa'' Programme for Centres of Excellence in R&D (MCIN, CEX2023-001286-S). E. L. S. acknowledges MECD, Spain, for a F. P. U. Fellowship.

Notes and references

1 M. Saito, H. Shinokubo and H. Sakurai, *Mater. Chem. Front.*, 2018, **2**, 635–661.
2 J. Martin, R. Slavchov, E. Yapp, J. Akroyd, S. Mosbach and M. Kraft, *J. Phys. Chem. C*, 2017, **121**, 27154–27163.
3 (*a*) L. Wang, D. Huang, L. Lam and Z. Cheng, *Liq. Cryst. Today*, 2017, **26**, 85–111; (*b*) M. J. Mayoral, J. Guilleme, J. Calbo, J. Aragó, F. Aparicio, E. Ortí, T. Torres and D. González-Rodríguez, *J. Am. Chem. Soc.*, 2020, **142**, 21017–21031; (*c*) J. Kang, D. Miyajima, T. Mori, Y. Inoue, Y. Itoh and T. Aida, *Science*, 2015, **347**, 646.
4 (*a*) D. Miyajima, K. Tashiro, F. Araoka, H. Takezoe, J. Kim, K. Kato, M. Takata and T. Aida, *J. Am. Chem. Soc.*, 2009, **131**, 44–45; (*b*) D. Miyajima, F. Araoka, H. Takezoe, J. Kim, K. Kato, M. Takata and T. Aida, *Science*, 2012, **336**, 209–213; (*c*) A. V. Gorbunov, M. G. Iglesias, J. Guilleme, T. D. Cornelissen, W. S. C. Roelofs, T. Torres, D. González-Rodríguez, E. W. Meijer and M. Kemerink, *Sci. Adv.*, 2017, **3**, e1701017; (*d*) S. Furukawa, J. Wu, M. Koyama, K. Hayashi, N. Hoshino, T. Takeda, Y. Suzuki, J. Kawamata, M. Saito and T. Akutagawa, *Nat. Commun.*, 2021, **12**, 768.
5 Y. Shoji, R. Komiyama, M. Kobayashi, A. Kosaka, T. Kajitani, R. Haruki, R. Kumai, S. Adachi, T. Tada, N. Karasawa, H. Nakano, H. Nakamura, H. Sakurai and T. Fukushima, *Sci. Adv.*, 2023, **9**, eadg8202.
6 (*a*) C. Zhang, K. Nakano, M. Nakamura, F. Araoka, K. Tajima and D. Miyajima, *J. Am. Chem. Soc.*, 2020, **142**, 3326–3330; (*b*) J. Guilleme, E. Cavero, T. Sierra, J. Ortega, C. L. Folcia, J. Etxebarría, T. Torres and D. González-Rodríguez, *Adv. Mater.*, 2015, **27**, 4280–4284; (*c*) J. Guilleme, J. Aragó, E. Ortí, E. Cavero, T. Sierra, J. Ortega, C. L. Folcia, J. Etxebarría, D. González-Rodríguez and T. Torres, *J. Mater. Chem. C*, 2015, **3**, 985–989; (*d*) M. Lehmann, M. Baumann, M. Lambov and A. Eremin, *Adv. Funct. Mater.*, 2021, **31**, 2104217.
7 (*a*) J. Labella and T. Torres, *Trends Chem.*, 2023, **5**, 353–366; (*b*) G. Lavarda, J. Labella, M. V. Martínez-Díaz, M. S. Rodríguez-Morgade, A. Osuka and T. Torres, *Chem. Soc. Rev.*, 2022, **51**, 9482.
8 (*a*) J. Labella, K. Shoyama, D. Guzmán, T. Schembri, M. Stolte, T. Torres and F. Würthner, *ACS Mater. Lett.*, 2023, **2**, 543–548; (*b*) J. Labella, J. Laforga-Martin and T. Torres, *CCS Chem.*, 2024, **6**, 276–296; (*c*) K. Cnops, B. P. Rand, D. Cheyns, B. Verreet, M. A. Empl and P. Heremans, *Nat. Commun.*, 2014, **5**, 4406/1–4406/6.
9 J. Labella, D. K. Bhowmick, A. Kumar, R. Naaman and T. Torres, *Chem. Sci.*, 2023, **14**, 4273–4277.
10 (*a*) E. van de Winckel, M. Mascaraque, A. Zamarrón, Á. Juarranz de la Fuente, T. Torres and A. de la Escosura,

Adv. Funct. Mater., 2018, **28**, 1705938; (*b*) J. Demuth, L. Gallego, M. Kozlikova, M. Machacek, R. Kucera, T. Torres, M. Martinez-Diaz and V. Novakova, *J. Med. Chem.*, 2021, **64**, 17436–17447.

11 (*a*) H. Gotfredsen, D. Thiel, P. M. Greißel, L. Chen, M. Krug, I. Papadopoulos, M. J. Ferguson, M. B. Nielsen, T. Torres, T. Clark, D. M. Guldi and R. R. Tykwinski, *J. Am. Chem. Soc.*, 2023, **145**, 9548–9563; (*b*) G. Lavarda, J. Zirzlmeier, M. Gruber, P. R. Rami, R. R. Tykwinski, T. Torres and D. M. Guldi, *Angew. Chem., Int. Ed.*, 2018, **57**, 16291–16295.

12 J. Labella, G. Lavarda, L. Hernández-López, F. Aguilar-Galindo, S. Díaz-Tendero, J. Lobo-Checa and T. Torres, *J. Am. Chem. Soc.*, 2022, **144**, 16579–16587.

13 (*a*) L. T. Scott, M. M. Hashemi and M. S. Bratcher, *J. Am. Chem. Soc.*, 1992, **114**, 1920–1921; (*b*) T. Amaya, H. Sakane, T. Muneishi and T. Hirao, *Chem. Commun.*, 2008, 765–767.

14 M. Gómez-Gómez, J. Labella and T. Torres, *Chem. – Eur. J.*, 2023, **29**, e202301782.

15 J. Labella, E. López-Serrano, D. Aranda, M. J. Mayoral, E. Ortí and T. Torres, *Chem. Sci.*, 2024, **15**, 13760–13767.